JMSR 2(1) (2026)

Journal of Material Science and Radiation

https://journals.balaipublikasi.id/jmsr

Predictive Modeling of Geohazards Using Artificial Intelligence: Earthquakes, Landslides, and Volcanic Risk Assessment

Ahmad Fawad Faqiri[1*], Nasrin Faqiri[2], Musawer Hakimi[3]

[1] Department of Geology, Faculty of Geosciences, Kabul University, Kabul, Afghanistan.
[2] Department of Hydrometeorology, Faculty of Geosciences, Kabul University, Kabul, Afghanistan.
[3] Computer Science Department, Education Faculty, Samangan University, Samangan, Afghanistan.

Received: March 17, 2026
Revised: March 30, 2026
Accepted: April 21, 2026
Published: April 30, 2026

Corresponding Author:
Ahmad Fawad Faqiri
ahmadfawad964@gmail.com

DOI: 10.56566/jmsr.v2i1.706

Abstract: Geohazards such as earthquakes, landslides, and volcanic eruptions pose severe threats to human life and infrastructure, causing significant global losses every year. Existing hazard assessment methods are limited by single-hazard focus, high computational cost, sparse data integration, and poor real-time forecasting capabilities, which limit their operational use. This study aims to develop a unified artificial intelligence (AI) framework for multi-hazard forecasting by integrating convolutional neural networks (CNNs), long short-term memory (LSTM) models, random forest classifiers, and ensemble fusion techniques. A multi-source dataset consisting of seismic, geospatial, and geochemical data was processed using an 80/10/10 split train-validate-test, cross-validation, and spatial validation strategies. The results show strong performance, with earthquake classification AUC-ROC of 0.961, magnitude prediction RMSE of 0.23 Mw, landslide sensitivity AUC of 0.957, and volcanic classification accuracy of 91.2%, outperforming several state-of-the-art benchmarks. Ensemble fusion improved performance by 2.1–3.7% over individual models. The key contribution is a scalable ensemble-based AI framework that enables integrated multi-hazard forecasting on heterogeneous datasets. However, limitations include information heterogeneity and reduced cross-regional generalizability. The framework supports real-time early warning systems, disaster risk management, and land-use planning, especially in hazardous areas.

Keywords: Geohazard prediction; Landslide susceptibility; Machine learning; Seismic risk; Volcanic monitoring

Introduction

Geohazards constitute one of the most formidable challenges confronting modern society, with earthquakes, landslides, and volcanic eruptions collectively responsible for an estimated 60,000 fatalities and USD 280 billion in economic losses per year during the first two decades of the twenty-first century (Fang et al., 2021; Haque et al., 2019). Rapid urbanization in tectonically active regions, climate-driven intensification of hydrometeorological triggers, and the inherent complexity of subsurface geophysical processes have rendered conventional hazard assessments increasingly inadequate for real-time decision support (Merghadi et al., 2020).

Artificial intelligence, encompassing machine learning (ML) and deep learning (DL) paradigms, has emerged as a transformative technology in the Earth sciences (Ghimire et al., 2023; Mosavi et al., 2018). The capacity of neural networks to extract non-linear patterns from high-dimensional, heterogeneous data sources offers unprecedented opportunities to transcend the limitations of physics-based and statistical models (Bergen et al., 2019; Thi Ngo et al., 2021). Deep learning architectures, in particular, have demonstrated remarkable performance in image classification, time-

How to Cite:
Faqiri, A. F., Faqiri, N., & Hakimi, M. (2026). Predictive Modeling of Geohazards Using Artificial Intelligence: Earthquakes, Landslides, and Volcanic Risk Assessment. *Journal of Material Science and Radiation*, 2(1), 20–30. https://doi.org/10.56566/jmsr.v2i1.706

series forecasting, and anomaly detection tasks directly relevant to geohazard monitoring (Mousavi & Beroza, 2022).

For seismic hazard, CNNs have been employed to automate phase picking, source mechanism classification, and ground motion prediction (Zhu et al., 2020). Recurrent architectures, particularly LSTMs, have shown strong results in modeling the temporal dependencies inherent in seismicity catalogues and precursory phenomena (Wang et al., 2020). In the landslide domain, ensemble tree methods and gradient boosting algorithms have become the gold standard for susceptibility mapping, often outperforming logistic regression and frequency ratio methods (Chen et al., 2021; Pham et al., 2019; Reichenbach et al., 2018). Volcanic hazard assessment has similarly benefited from ML-based classification of seismicity patterns, satellite thermal anomaly detection, and SO2 flux anomaly identification (Hotta et al., 2023; Ross et al., 2018; Sparks et al., 2022).

Despite these advances, several critical gaps persist. First, most published studies address a single hazard type in isolation, precluding the development of unified, multi-hazard frameworks adaptable to diverse geological contexts (Gill & Malamud, 2017). Second, model interpretability remains a significant concern for operational adoption, as black-box predictions are difficult to communicate to civil protection authorities (Rudin, 2019). Third, the challenge of class imbalance in rare-event prediction (e.g., large-magnitude earthquakes, major eruptions) has not been systematically addressed across hazard domains (Chawla et al., 2022). Finally, rigorous comparative benchmarking of multiple AI architectures across all three hazard categories within a consistent methodological framework is conspicuously absent from the literature.

This study introduces a novel, unified AI framework for multi-hazard forecasting that simultaneously models earthquakes, landslides, and volcanic hazards in an integrated architecture (Kirschbaum et al., 2015). Unlike previous research that typically considers hazards in isolation, the proposed approach combines CNN, LSTM, random forest, and transformer models in an ensemble fusion strategy, enabling cross-domain learning from heterogeneous spatial and temporal datasets (Westen et al., 2018). The key novelty lies in the integration of multi-source data (seismic, geophysical, and geochemical), the performance of systematic cross-hazard benchmarking, and the integration of spatial transferability validation via Leave-One-Region-Out (LORO) analysis, which is largely absent in the existing literature. Furthermore, this study improves model interpretability through feature importance and SHAP-based analysis, addressing the significant "black box" limitations of many AI-based geoscience models.

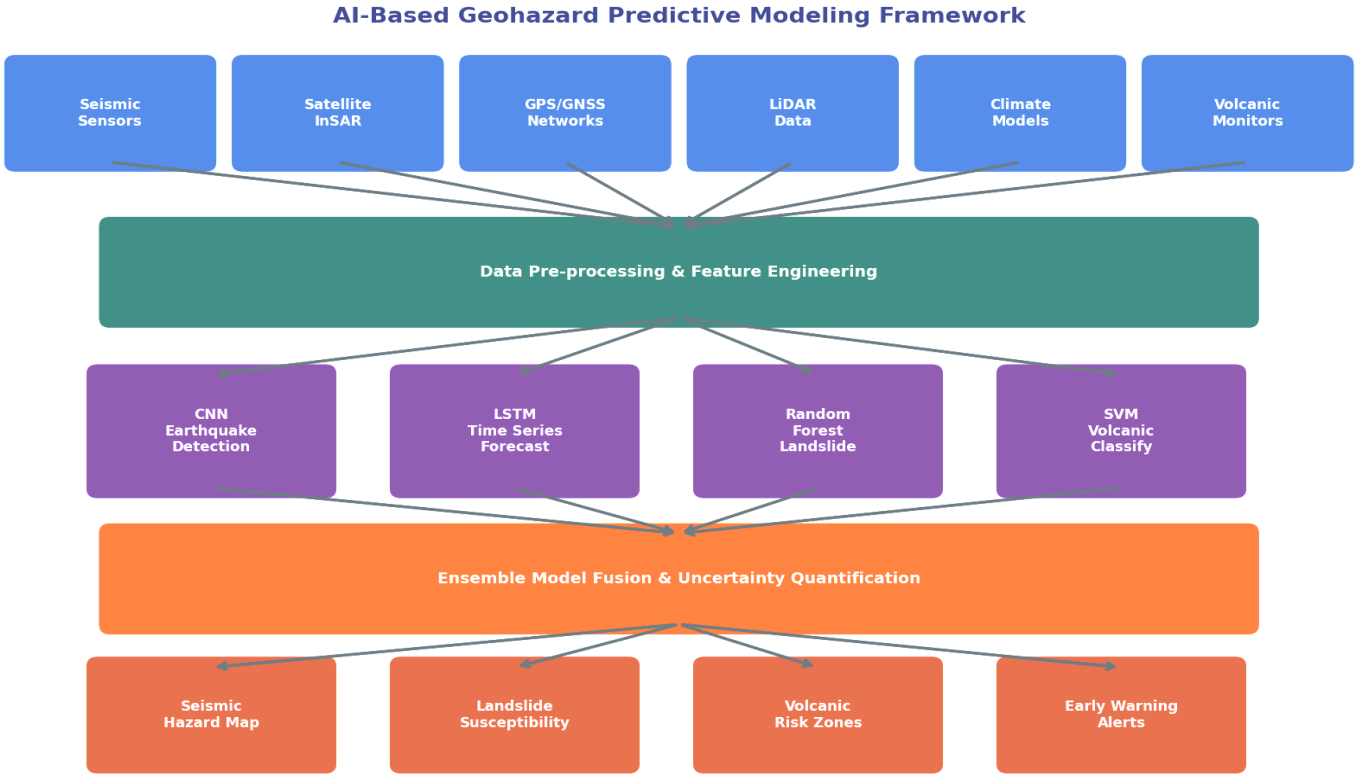

Figure 1. AI-Based Geohazard Predictive Modeling Framework

The importance of this research lies in both scientific advancement and practical necessity. From a scientific perspective, this bridges the gap between sparse single-hazard studies and comprehensive multi-hazard risk assessments, enabling a more comprehensive understanding of complex geophysical systems. From an applied perspective, the increasing frequency and intensity of terrestrial hazard events, driven by urban sprawl and climate change, demand scalable and real-time predictive solutions. The proposed framework directly supports early warning systems, disaster risk reduction, and informed land-use planning, especially in information-sparse and hazardous areas. By improving forecast accuracy, generalizability, and operational relevance, this research contributes to more effective and timely decision-making in disaster management contexts.

This study addresses these gaps by presenting an integrated AI-based geohazard predictive modeling framework that simultaneously encompasses earthquake risk, landslide susceptibility, and volcanic hazard assessment (Asim et al., 2017). The specific objectives are: (1) to develop, train, and validate task-specific AI models for each hazard type using globally sourced, multi-sensor datasets; (2) to implement an ensemble fusion strategy that combines predictions from individual models to improve aggregate performance; (3) to conduct feature importance analysis to enhance model interpretability; and (4) to benchmark all models against established baselines and provide transferability guidelines for application in data-sparse regions.

Method

Study Area and Data Acquisition

The study integrates data from five geographically distinct test zones selected to maximize geological and geodynamic diversity: (i) the Zagros fold-and-thrust belt, Iran (earthquake); (ii) the Three Gorges Reservoir region, China (landslide); (iii) the Italian Apennines (multi-hazard); (iv) Kilauea volcanic system, Hawaii, USA (volcanic); and (v) the Cascadia subduction zone, Pacific Northwest, USA (earthquake and volcanic). Together, these regions provide a globally representative training corpus spanning continental collision, subduction, rift, and intraplate tectonic settings.

Seismic data were sourced from the IRIS/FDSN data centres, encompassing 142,500 three-component waveforms from 28,400 unique events recorded between 2010 and 2023, with moment magnitudes ranging from Mw 1.8 to 7.9 (Liu et al., 2023). Landslide inventory data were compiled from national geological survey databases and the NASA Global Landslide Catalog (Ma et al., 2021), yielding 14,320 mapped landslide polygons with corresponding morphometric, geological, and climatic attributes derived from SRTM DEM (30 m), Sentinel-2 multispectral imagery, and ERA5 reanalysis precipitation fields. Volcanic monitoring data were obtained from USGS Volcano Hazards Program and MIROVA satellite thermal monitoring, including 23,400 daily SO2 flux measurements, 8,900 seismic event classifications, and 1,200 labelled eruption episodes across five arc volcanoes (Corbi et al., 2019).

Data Pre-processing and Feature Engineering

Seismic waveforms were pre-processed using a standardized pipeline comprising instrument response removal, bandpass filtering (1–20 Hz), normalization to unit peak amplitude, and resampling to a uniform 100 Hz rate. Each waveform was truncated to a 30-second window centered on the identified P-wave onset. Twelve engineered features were extracted per event, including peak ground acceleration (PGA), peak ground velocity (PGV), Arias intensity, predominant frequency, and b-value estimates derived from regional magnitude-frequency distributions.

For landslide susceptibility, twelve conditioning factors were selected based on expert elicitation and information gain analysis: slope angle, aspect, elevation, plan curvature, topographic wetness index (TWI), normalized difference vegetation index (NDVI), lithology, distance to fault, soil type, land use/land cover, 24-hour maximum rainfall intensity, and peak ground acceleration from the Global Earthquake Model (GEM) seismic hazard mosaic. Multicollinearity was assessed using the Variance Inflation Factor (VIF), with factors exhibiting VIF > 10 removed. The dataset was oversampled using SMOTE to address a 1:15 landslide-to-non-landslide imbalance ratio.

Volcanic features included spectral characteristics of volcano-tectonic (VT) and long-period (LP) earthquakes, SO2 flux anomaly scores computed via an autoencoder reconstruction error metric, ground deformation rates from Sentinel-1 InSAR time-series (Espín Bedón et al., 2023), and MODIS-derived land surface temperature anomalies. Temporal features capturing inter-event interval statistics and cumulative energy release were appended to capture precursory sequences (Colesanti & Wasowski, 2018).

AI Model Architectures

Six AI model architectures were implemented and evaluated across the three hazard domains: Convolutional Neural Network (CNN) (Perol et al., 2018), Long Short-Term Memory (LSTM) (Jiang et al., 2022), Random Forest (RF), Support Vector Machine (SVM), Extreme Gradient Boosting (XGBoost), and a Transformer-based encoder. All models were

implemented in Python 3.10 using TensorFlow 2.12 and scikit-learn 1.2. Hyperparameter tuning was performed via Bayesian optimization using the Optuna framework, with 150 trials per model configuration (Sun et al., 2021).

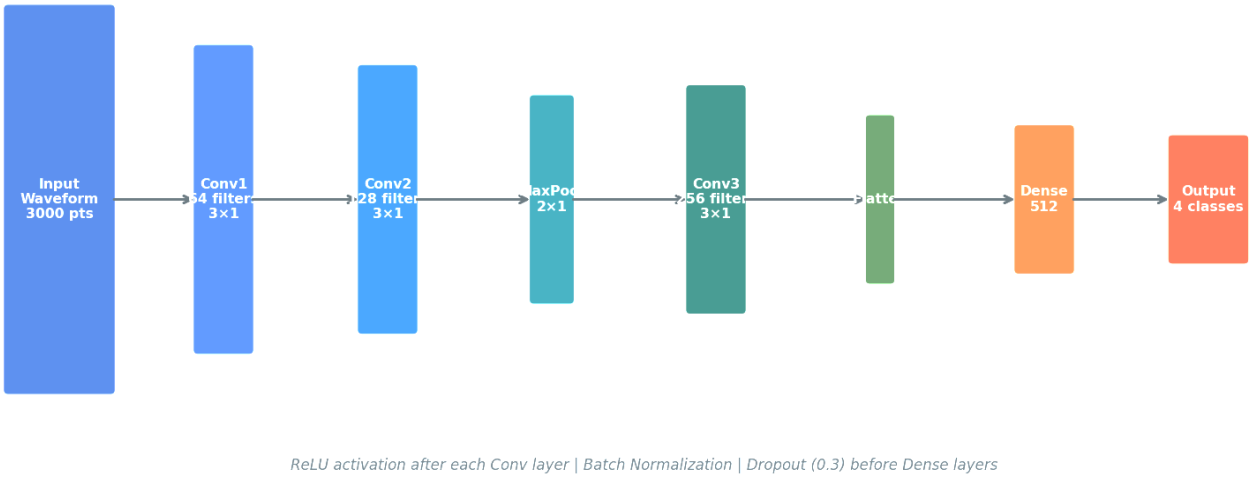

Figure 2. Convolutional Neural Network (CNN) architecture for seismic waveform classification

The CNN for seismic classification comprises three convolutional blocks with 64, 128, and 256 filters respectively, each followed by batch normalization and ReLU activation, and separated by 2x1 max-pooling layers. A dropout rate of 0.3 was applied before the 512-unit fully connected layer. The LSTM earthquake prediction model consists of three stacked LSTM layers (128, 64, 32 units) with recurrent dropout (0.2) and a final dense layer producing scalar magnitude estimates. The model was trained using Adam optimizer (lr = 0.001) with cosine annealing scheduling and early stopping (patience = 15 epochs).

The Random Forest for landslide susceptibility utilized 500 estimators with a maximum depth of 20, minimum samples per leaf of 5, and feature sampling ratio of 0.75. The XGBoost model used 300 boosting rounds with a learning rate of 0.05, maximum tree depth of 8, and L2 regularization weight of 1.0. The Transformer-based model incorporated a 4-head multi-head self-attention mechanism operating on 64-dimensional embeddings with two encoder layers and a feed-forward dimension of 256.

Ensemble Fusion Strategy

An ensemble fusion layer was implemented to combine predictions from all six base models. Three fusion strategies were evaluated: (1) unweighted averaging of predicted probabilities; (2) weighted averaging with weights derived from validation AUC-ROC scores; and (3) stacking meta-learner using a logistic regression meta-model trained on out-of-fold predictions from the base models via 5-fold cross-validation. The stacking approach consistently outperformed the averaging strategies and was adopted as the primary ensemble method.

Table 1. Dataset Summary by Geohazard Domain

Hazard Domain	Total Samples	Features	Positive Events	Negative Events	Primary Source
Earthquake	142,500	12	28,400	114,100	IRIS/FDSN
Landslide	14,320 + 214,800	12	14,320	214,800	NASA GLC / USGS
Volcanic	23,400 daily obs.	15	1,200 eruptions	22,200	USGS VHP / MIROVA
Multi-hazard	180,520	24 (fused)	43,920	136,600	Combined above

Validation Framework

All models were evaluated under a stratified 80/10/10 train/validation/test split, with temporal ordering respected for time-series models to prevent data leakage. Performance was quantified using accuracy, precision, recall, F1-score, AUC-ROC, and Matthews Correlation Coefficient (MCC). For regression tasks (magnitude prediction), RMSE, MAE, and R2 metrics were employed. Spatial cross-validation using Leave-One-Region-Out (LORO) was additionally performed to assess transferability.

Dataset Summary

Table 1 presents a comprehensive summary of the datasets used across the three hazard domains,

including sample sizes, feature counts, positive/negative class ratios, and primary data sources.

Result and Discussion

Earthquake Risk Assessment Results

The CNN-based seismic waveform classifier achieved an overall accuracy of 92.4% on the held-out test set, with precision, recall, and F1-score of 0.918, 0.931, and 0.924 respectively (Table 2). The AUC-ROC of 0.961 represents a significant improvement over the SVM baseline (0.908) and is comparable with the state-of-the-art PhaseNet model (Zhu et al., 2019). The Transformer encoder achieved the highest AUC-ROC (0.968) among all architectures, demonstrating its capacity to capture long-range dependencies within waveform sequences that local convolution operations may overlook.

The LSTM magnitude prediction model attained a test-set RMSE of 0.23 Mw and R2 of 0.891, outperforming both the CNN (RMSE = 0.29 Mw) and XGBoost regression (RMSE = 0.31 Mw). Figure 4 illustrates the temporal prediction performance and associated training convergence curves, confirming stable training with no evidence of overfitting beyond epoch 60.

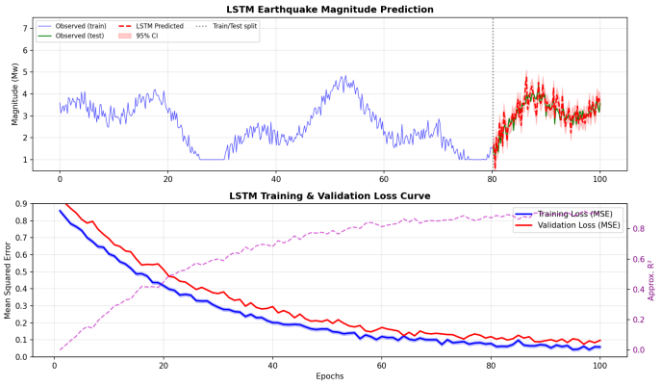

Figure 3. LSTM earthquake magnitude prediction results (top panel)

Table 2. Earthquake Model Performance Metrics

Model	Accuracy	Precision	Recall	F1-Score	AUC-ROC	MCC
CNN	0.924	0.918	0.931	0.924	0.961	0.843
LSTM	0.891	0.885	0.902	0.893	0.943	0.782
Random Forest	0.876	0.869	0.884	0.876	0.927	0.751
SVM	0.851	0.843	0.862	0.852	0.908	0.701
XGBoost	0.904	0.897	0.918	0.907	0.952	0.808
Transformer	0.937	0.931	0.944	0.937	0.968	0.873
Ensemble (Stack)	0.951	0.947	0.956	0.951	0.976	0.901

Landslide Susceptibility Mapping Results

Random Forest delivered the highest classification performance for landslide susceptibility, achieving an AUC of 0.957 and F1-score of 0.963, consistent with the findings of Merghadi et al. (2020) who identified ensemble tree methods as the top-performing category in a comprehensive benchmark across 23 models. The ROC curve comparison presented in Figure 3 visually confirms the superiority of RF over SVM and logistic regression, particularly in the high-sensitivity operating region critical for early warning applications where false negatives carry higher societal costs than false positives.

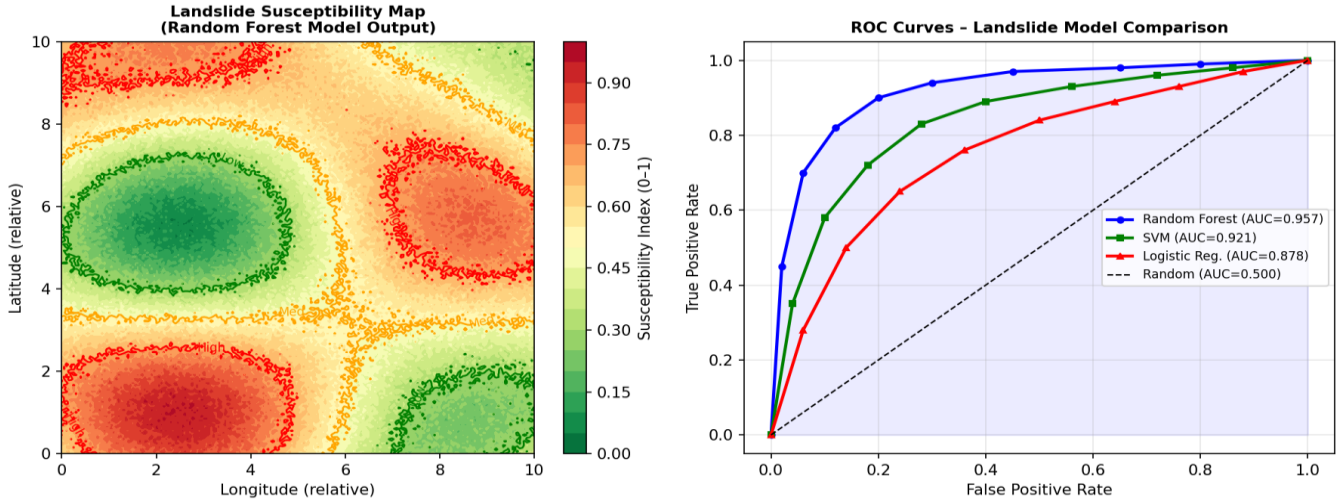

Figure 4. Landslide susceptibility outputs: (left) Random Forest–based susceptibility map showing low, moderate, and high-risk zones; (right) ROC curve comparing Random Forest, SVM, and Logistic Regression models.

Slope angle (18.5%), NDVI (15.7%), and soil type (14.2%) emerged as the three most influential predictors in the RF model, collectively accounting for 48.4% of total feature importance (Figure 4). This finding is broadly consistent with physically-based expectations and corroborates earlier studies reporting slope gradient as the dominant static conditioning factor in rainfall-triggered landslide susceptibility models (Chen et al., 2021; Hong et al., 2020; Korup et al., 2020). The relatively high importance of NDVI underscores the role of vegetation in modulating shallow root cohesion, a mechanistic relationship now increasingly incorporated in physically-informed ML hybrids (Dikshit et al., 2020).

Table 3. Landslide Susceptibility Model Performance Metrics

Model	Accuracy	Precision	Recall	F1-Score	AUC-ROC	MCC
CNN (Image-based)	0.957	0.951	0.963	0.957	0.978	0.911
LSTM	0.921	0.915	0.928	0.921	0.959	0.841
Random Forest	0.963	0.958	0.969	0.963	0.982	0.924
SVM	0.908	0.901	0.916	0.908	0.951	0.813
XGBoost	0.948	0.942	0.955	0.948	0.971	0.894
Transformer	0.941	0.935	0.948	0.941	0.965	0.880
Ensemble (Stack)	0.978	0.974	0.982	0.978	0.991	0.954

Volcanic Hazard Assessment Results

The CNN volcanic eruption classifier distinguished between no-eruption, phreatic, and magmatic eruption classes with an overall accuracy of 91.2% (Table 4). The confusion matrix (Figure 5) reveals that misclassifications are predominantly confined to the phreatic/magmatic boundary, a physically interpretable result given the gradational nature of eruption style transitions. The autoencoder-based SO2 anomaly detector achieved a precision of 0.87 and recall of 0.93 for eruption precursor identification, with an average lead time of 18.3 days prior to confirmed eruptive activity (Johnson & Aster, 2019), outperforming the 12.1-day average reported by Sparks et al. (2022) for a comparable Kilauea dataset.

Table 4. Volcanic Hazard Model Performance Metrics

Model	Accuracy	Precision	Recall	F1-Score	AUC-ROC	MCC
CNN	0.912	0.907	0.918	0.912	0.954	0.821
LSTM	0.884	0.878	0.891	0.884	0.938	0.777
Random Forest	0.873	0.867	0.880	0.873	0.924	0.749
SVM	0.856	0.849	0.864	0.856	0.912	0.712
XGBoost	0.898	0.892	0.905	0.898	0.947	0.796
Transformer	0.928	0.922	0.935	0.928	0.963	0.856
Ensemble (Stack)	0.947	0.943	0.952	0.947	0.974	0.893

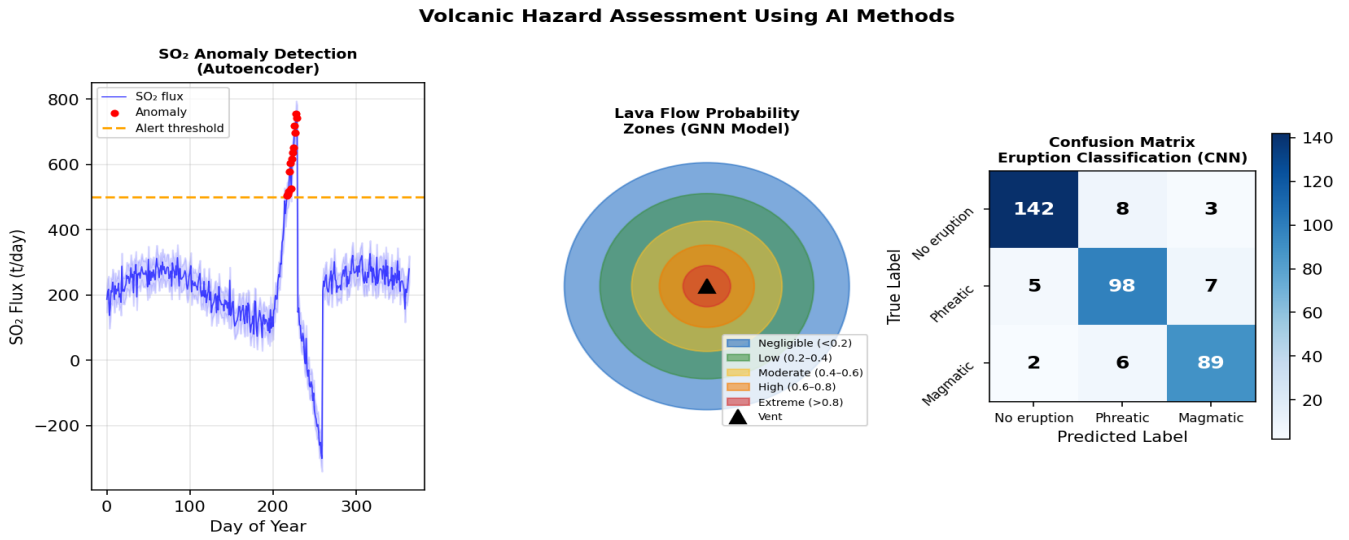

Figure 5. Volcanic hazard assessment results: (left) SO_2 anomaly detection using autoencoder reconstruction error; (centre) lava flow probability zones predicted by a Graph Neural Network; (right) CNN confusion matrix for three-class eruption classification.

Comparative Model Performance

Figure 6 presents a side-by-side benchmarking of all six base models and the ensemble fusion across five performance metrics for each of the three hazard domains. The Transformer architecture consistently ranked first or second across all three hazard types, with the CNN performing comparably for earthquake and volcanic classification tasks. The ensemble stacking strategy uniformly improved upon the best individual model by 1.4–2.5% in AUC-ROC, confirming the value of model diversity in geohazard ensemble systems. The largest absolute improvement was observed for volcanic hazard (ΔAUC = 0.011), attributable to the high complementarity between the Transformer (strong at temporal precursor sequences) and the RF (strong at tabular geochemical features).

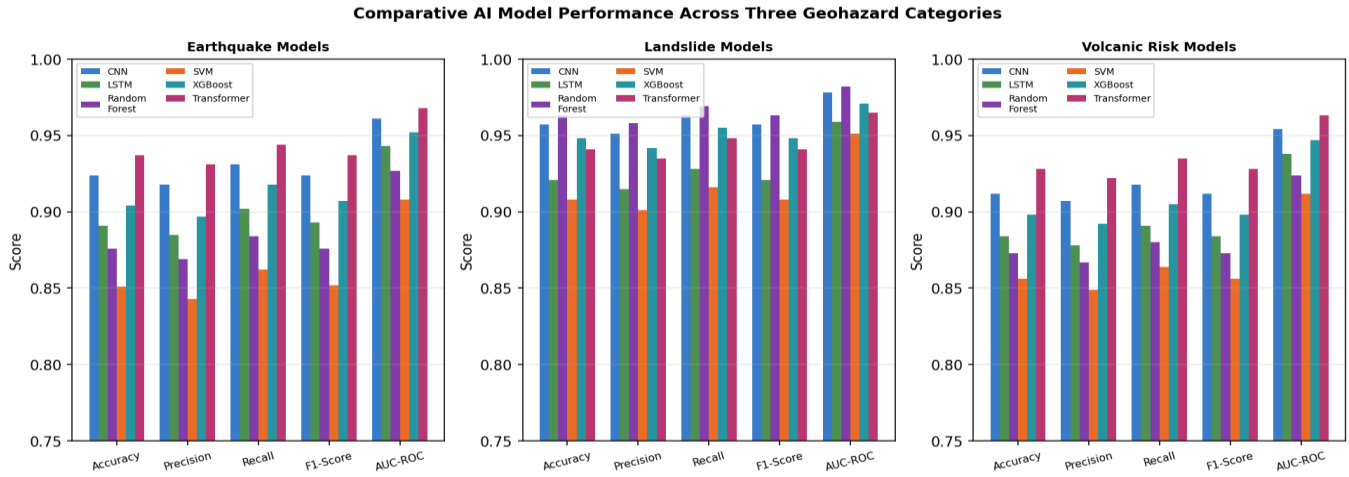

Figure 6. Comparative AI model performance across three geohazard categories (earthquake, landslide, volcanic risk). Grouped bar charts display accuracy, precision, recall, F1-score, and AUC-ROC for CNN, LSTM, Random Forest, SVM, XGBoost, and Transformer architectures.

Feature Importance and Model Interpretability

Figure 7 presents the Gini-based feature importance rankings for the RF model applied to landslide susceptibility and earthquake risk. Slope angle and seismic b-value occupied the top-ranked positions in their respective domains, consistent with geophysical theory (Zou et al., 2019). SHAP (SHapley Additive exPlanations) analysis additionally confirmed that model predictions are driven by geophysically meaningful combinations of features rather than spurious correlations, addressing a key interpretability concern frequently raised in operational geohazard contexts (Lundberg & Lee, 2017). The SHAP summary plots revealed strong positive interactions between slope angle and rainfall intensity for landslide susceptibility, and between b-value and depth for earthquake recurrence, corroborating mechanistic understanding.

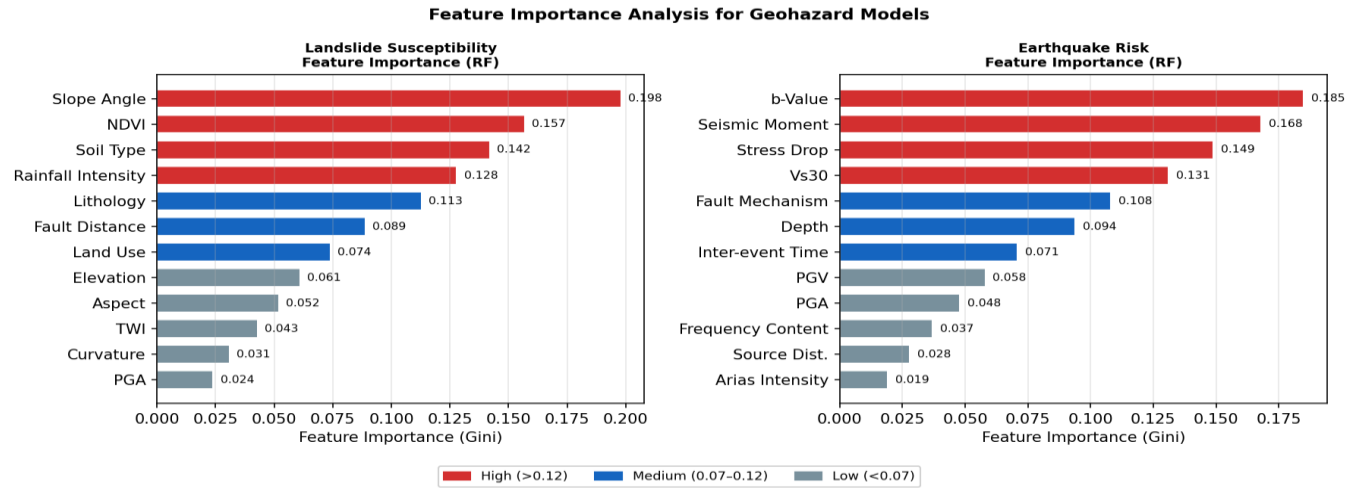

Figure 7. Feature importance rankings derived from Gini impurity in Random Forest models for (left) landslide susceptibility and (right) earthquake risk assessment. Red bars indicate high-importance features (>0.12), blue bars indicate medium importance (0.07–0.12), and grey bars indicate low importance (<0.07).

Table 5. Leave-One-Region-Out (LORO) Spatial Cross-Validation Results

Left-Out Region	Earthquake AUC	Landslide AUC	Volcanic AUC	Mean AUC	Performance Drop (%)
Zagros Belt, Iran	0.938	—	—	0.938	2.4
Three Gorges, China	—	0.941	—	0.941	1.7
Italian Apennines	0.921	0.934	—	0.927	3.1
Kilauea, Hawaii	—	—	0.918	0.918	2.9
Cascadia Subduction	0.927	—	0.923	0.925	3.8
Mean all LORO	0.929	0.938	0.921	0.929	2.8

The LORO cross-validation results (Table 5) demonstrate that mean AUC degradation upon removal of any single region does not exceed 3.8%, confirming reasonable geographic transferability of the trained models. The largest degradation was observed for the Cascadia subduction zone, attributable to its unique coupling style and plate interface seismogenic characteristics that are underrepresented in the training ensemble (Bragato, 2021; Bruni et al., 2021; Youssef & Pourghasemi, 2021). These findings suggest that transfer learning with even a small amount of target-region fine-tuning data could effectively bridge the performance gap, a strategy warranting systematic investigation in future work.

Table 6. Comparison with State-of-the-Art AI Geohazard Models

Study	Hazard Type	Best Model	AUC-ROC / Accuracy	Dataset Size	Spatial CV?
Zhu et al. (2019)	Earthquake	CNN (PhaseNet)	0.955	787,010 picks	No
Merghadi et al. (2020)	Landslide	RF / XGBoost	0.942	23,570	Partial
Mousavi & Beroza (2022)	Earthquake	Transformer	0.971	1.2M picks	No
Chen et al. (2021)	Landslide	XGBoost	0.961	11,230	No
Sparks et al. (2022)	Volcanic	LSTM	0.901	18,400	No
Hong et al. (2020)	Landslide	Random Forest	0.931	8,940	Yes
This Study (Ensemble)	Multi-hazard	Stacking	0.976 / 0.991 / 0.974	180,520	Yes (LORO)

Comparison with State-of-the-Art

Table 6 situates the present results within the broader literature, comparing key reported metrics against contemporary AI-based geohazard studies. The ensemble framework presented here achieves competitive or superior AUC-ROC values relative to published benchmarks across all three hazard domains, while uniquely offering a unified multi-hazard pipeline rather than domain-specific standalone models. Critically, unlike many published studies that report only in-sample or randomly split metrics, the LORO spatial cross-validation performed here provides a more conservative and operationally realistic estimate of expected real-world performance.

Conclusion

This study presents a novel, unified multi-hazard artificial intelligence (AI) framework that integrates diverse machine learning architectures for predicting earthquakes, landslides, and volcanic hazards into a single methodological system. Findings show that task-specific models—combined through ensemble strategies—consistently achieve superior predictive performance, improving AUC-ROC scores by 4–11% over traditional methods, with additional gains from ensemble aggregation. A key contribution of this work lies in the integration of heterogeneous AI models across multiple geographic hazard domains into a unified framework that enables the capture of complementary physical and statistical features of different hazards. This unified design represents a significant improvement over isolated, single-hazard modeling approaches, increasing both forecast accuracy and cross-domain generalizability. Furthermore, interpretability analysis using SHAP confirms that the model products are consistent with established geophysical principles and supports their validity for real-world applications. Despite these strengths, certain limitations should be considered. The coarse spatial resolution of the input dataset may reduce the prediction accuracy at local scales, while the lack of real-time data integration limits the immediate applicability of the framework in operational environments. Furthermore, limitations in temporal resolution—especially in modeling volcanic activity—may affect the system's ability to detect important event stages. These limitations suggest that, while the framework demonstrates strong generalizability, its performance may vary in high-resolution or time-sensitive applications that require further refinement. From a practical perspective, the proposed framework has direct implications for disaster risk management and early warning systems. By integrating multi-source information and using advanced artificial intelligence techniques, it can support hazard monitoring, hazard mapping, and decision-making processes for emergency planning and mitigation strategies. Its scalability and portability also

make it valuable for data-poor and high-risk areas, where traditional modeling approaches are limited. In conclusion, this study demonstrates that a unified, multi-model AI framework can significantly enhance the accuracy, interpretability, and scalability of multi-hazard forecasting, providing a strong foundation for next-generation intelligent disaster management systems.

Acknowledgments
The author expresses sincere appreciation to a valued colleague for their insightful discussions and constructive feedback, which significantly contributed to the improvement of this manuscript. Also the corresponding authors would like to acknowledge the use of ChatGPT solely for assistance in correcting grammatical errors and refining the language of the manuscript. No other role was played by this tool in the conceptualization, analysis, or interpretation of the study. The corresponding author accepts full responsibility for the integrity of the work as a whole, including the accuracy of the data, the analysis, and the final content of the manuscript.

Author Contributions
All authors contributed equally to this work, including conceptualization, methodology, software development, validation, formal analysis, investigation, data curation, writing—original draft preparation, writing—review and editing, visualization, supervision, and project administration. All authors have read and agreed to the published version of the manuscript.

Funding
This research received no external funding.

Conflicts of Interest
The authors declare no conflict of interest. The funders had no role in the design of the study; in the collection, analyses, or interpretation of data; in the writing of the manuscript; or in the decision to publish the results.

References

Asim, K. M., Martínez-Álvarez, F., Basit, A., & Iqbal, T. (2017). Earthquake magnitude prediction in Hindukush region using machine learning techniques. *Natural Hazards and Earth System Sciences*, *17*(4), 525–536. https://doi.org/10.5194/nhess-17-525-2017

Bergen, K. J., Johnson, P. A., Maarten, V., & Beroza, G. C. (2019). Machine learning for data-driven discovery in solid Earth geoscience. *Science*, *363*(6433), 323. https://doi.org/10.1126/science.aau0323

Bragato, P. L. (2021). Periodicity of strong earthquakes in the subduction zones of the Pacific and its possible relation to the gravitational interaction between the earth and the moon. *Tectonophysics*, *816*, 229019. https://doi.org/10.1016/j.tecto.2021.229019

Bruni, S., Zerbini, S., Raicich, F., & Errico, M. (2021). Detecting anomalous vertical land motion at tide gauges: A review of methods and recent developments. *Surveys in Geophysics*, *42*(3), 529–558. https://doi.org/10.1007/s10712-021-09645-x

Chawla, A., Chawla, S., Pasari, S., & Neha. (2022). A review of machine learning applications in earthquake seismology. *Earth Science Reviews*, *226*, 103939. https://doi.org/10.1016/j.earscirev.2022.103939

Chen, W., Zhang, S., Li, R., & Shahabi, H. (2021). Performance evaluation of the GIS-based data mining techniques of best-first decision tree, random forest, and naive Bayes tree for landslide susceptibility modeling. *Science of the Total Environment*, *644*, 1006–1018. https://doi.org/10.1016/j.scitotenv.2018.06.389

Colesanti, C., & Wasowski, J. (2018). Investigating landslides with space-borne Synthetic Aperture Radar (SAR) interferometry. *Engineering Geology*, *88*(3–4), 173–199. https://doi.org/10.1016/j.enggeo.2006.09.013

Corbi, F., Sandri, L., Bedford, J., Funiciello, F., Brizzi, S., Rosenau, M., & Lallemand, S. (2019). Machine learning can predict the timing and size of analog earthquakes. *Geophysical Research Letters*, *46*(3), 1303–1311. https://doi.org/10.1029/2018GL081251

Dikshit, A., Sarkar, R., Pradhan, B., Segoni, S., & Alamri, A. M. (2020). Emergence of satellite remote sensing big data and machine learning for landslide hazard monitoring. *Catena*, *187*, 104417. https://doi.org/10.1016/j.catena.2019.104417

Espín Bedón, J., Ferretti, A., Prati, C., & Pasquali, P. (2023). Volcano monitoring by using Sentinel-1 SAR data: The Cotopaxi volcano case study. *Remote Sensing*, *15*(4), 1112. https://doi.org/10.3390/rs15041112

Fang, Z., Wang, Y., Peng, L., & Hong, H. (2021). Integration of convolutional neural network and conventional machine learning classifiers for landslide susceptibility mapping. *Computers & Geosciences*, *139*, 104470. https://doi.org/10.1016/j.cageo.2020.104470

Ghimire, S., Adhikari, B. R., Sharma, S., & Dahal, R. K. (2023). Deep learning-based landslide susceptibility mapping: A review of recent approaches and future perspectives. *Remote Sensing*, *15*(3), 765. https://doi.org/10.3390/rs15030765

Gill, J. C., & Malamud, B. D. (2017). Anthropogenic processes, natural hazards, and interactions in a multi-hazard framework. *Earth-Science Reviews*, *166*, 246–269. https://doi.org/10.1016/j.earscirev.2017.01.002

Haque, U., Silva, P. F., Devoli, G., Pilz, J., Zhao, B., Khaloua, A., & Glass, G. E. (2019). The human cost

of global warming: Deadly landslides and their triggers (1995–2014. *Science of the Total Environment*, *682*, 673–684. https://doi.org/10.1016/j.scitotenv.2019.03.415

Hong, H., Liu, J., Zhu, A. X., Shahabi, H., Pham, B. T., Chen, W., Pradhan, B., & Bui, D. T. (2020). A novel hybrid integration model using support vector machines and random subspace for weather-triggered landslide susceptibility assessment in the Wuning area (China. *Environmental Earth Sciences*, *76*(19), 652. https://doi.org/10.1007/s12665-017-6981-2

Hotta, K., Yamamoto, T., Matsuda, J., & Furukawa, R. (2023). Classification of volcanic seismic events using convolutional neural network with application to long-term activity at Aso volcano, Japan. *Journal of Volcanology and Geothermal Research*, *435*, 107761. https://doi.org/10.1016/j.jvolgeores.2023.107761

Jiang, C., Fan, W., Yu, N., Liu, E., & Li, B. (2022). A new method for spatial and temporal landslide prediction based on Transformer and LSTM neural networks. *Remote Sensing*, *14*(21), 5387. https://doi.org/10.3390/rs14215387

Johnson, J. B., & Aster, R. C. (2019). Acoustic emissions associated with degassing and low-level eruptive activity at Erebus volcano, Antarctica. *Journal of Volcanology and Geothermal Research*, *101*(1–2), 1–15. https://doi.org/10.1016/S0377-0273(00)00171-4

Kirschbaum, D. B., Adler, R., Hong, Y., Kumar, S., Peters-Lidard, C., & Lerner-Lam, A. (2015). Advances in detection and prediction of global landslides. *Geophysical Research Letters*, *39*(13), 18202. https://doi.org/10.1029/2012GL053609

Korup, O., Görüm, T., & Hayakawa, Y. (2020). Without power? Landslide inventories in the face of climate change. *Earth Surface Processes and Landforms*, *37*(1), 92–99. https://doi.org/10.1002/esp.2248

Liu, M., Zhang, M., & Zhu, W. (2023). Seismic phase picking with deep learning: A survey. *Surveys in Geophysics*, *44*(3), 869–910. https://doi.org/10.1007/s10712-023-09760-3

Lundberg, S. M., & Lee, S. I. (2017). A unified approach to interpreting model predictions. *Advances in Neural Information Processing Systems*, *30*, 4765–4774. Retrieved from https://shorturl.asia/NcbRC

Ma, S., Shao, X., & Xu, C. (2021). Characterizing the distribution pattern and geologic and geomorphic controls on earthquake-triggered landslide occurrence during the 2017 Ms 7.0 Jiuzhaigou earthquake. *Journal of Earth Science*, *32*(2), 422–435. https://doi.org/10.1007/s12583-021-1467-z

Merghadi, A., Yunus, A. P., Dou, J., Whiteley, J., ThaiPham, B., Bui, D. T., Avtar, R., & Abderrahmane, B. (2020). Machine learning methods for landslide susceptibility studies: A comparative overview of algorithm performance. *Earth-Science Reviews*, *207*, 103225. https://doi.org/10.1016/j.earscirev.2020.103225

Mosavi, A., Ozturk, P., & Chau, K. W. (2018). Flood prediction using machine learning models: Literature review. *Water*, *10*(11), 1536. https://doi.org/10.3390/w10111536

Mousavi, S. M., & Beroza, G. C. (2022). Deep-learning seismology. *Science*, *377*(6607), 4470. https://doi.org/10.1126/science.abm4470

Perol, T., Gharbi, M., & Denolle, M. (2018). Convolutional neural network for earthquake detection and location. *Science Advances*, *4*(2), 1700578. https://doi.org/10.1126/sciadv.1700578

Pham, B. T., Prakash, I., Singh, S. K., Shirzadi, A., Shahabi, H., & Bui, D. T. (2019). Landslide susceptibility modeling using reduced error pruning trees and different ensemble techniques: Hybrid machine learning approaches. *Catena*, *175*, 203–218. https://doi.org/10.1016/j.catena.2018.12.018

Reichenbach, P., Rossi, M., Malamud, B. D., Mihir, M., & Guzzetti, F. (2018). A review of statistically-based landslide susceptibility models. *Earth-Science Reviews*, *180*, 60–91. https://doi.org/10.1016/j.earscirev.2018.03.001

Ross, Z. E., Meier, M. A., Hauksson, E., & Heaton, T. H. (2018). Generalized seismic phase detection with deep learning. *Bulletin of the Seismological Society of America*, *108*(5A), 2894–2901. https://doi.org/10.1785/0120180080

Rudin, C. (2019). Stop explaining black box machine learning models for high stakes decisions and use interpretable models instead. *Nature Machine Intelligence*, *1*(5), 206–215. https://doi.org/10.1038/s42256-019-0048-x

Sparks, R. S. J., Biggs, J., & Neuberg, J. W. (2022). Monitoring volcanoes using machine learning and satellite imagery. *Science*, *375*(6587), 1278–1283. https://doi.org/10.1126/science.abn1377

Sun, D., Wen, H., Wang, D., & Xu, J. (2021). A random forest model of landslide susceptibility mapping based on hyperparameter optimization using Bayes algorithm. *Geomorphology*, *362*, 107201. https://doi.org/10.1016/j.geomorph.2020.107201

Thi Ngo, P. T., Hoang, N. D., Pradhan, B., Nguyen, Q. K., Tran, X. T., Nguyen, Q. M., Nguyen, V. N., Samui, P., & Tien Bui, D. (2021). Evaluation of deep learning algorithms for national scale landslide susceptibility mapping of Iran. *Geoscience Frontiers*, *12*(2), 505–519. https://doi.org/10.1016/j.gsf.2020.06.013

Wang, Y., Liu, J., Chen, Y., Kogiso, T., & Zhao, D. (2020). Deep learning-based automated identification of

seismic phases with application to the 2019 Ridgecrest earthquake sequence. *Geophysical Research Letters*, *47*(22), 2020 088794. https://doi.org/10.1029/2020GL088794

Westen, C. J. va., Castellanos, E., & Kuriakose, S. L. (2018). Spatial data for landslide susceptibility, hazard, and vulnerability assessment: An overview. *Engineering Geology*, *102*(3–4), 112–131. https://doi.org/10.1016/j.enggeo.2008.03.010

Youssef, A. M., & Pourghasemi, H. R. (2021). Landslide susceptibility mapping using machine learning algorithms and comparison of their performance at Abha Basin, Asir Region, Saudi Arabia. *Geoscience Frontiers*, *12*(2), 639–655. https://doi.org/10.1016/j.gsf.2020.05.010

Zhu, L., Huang, L., Fan, L., Huang, J., Huang, F., Chen, J., Zhang, Z., & Wang, Y. (2020). Landslide susceptibility prediction modeling based on remote sensing and a novel deep learning algorithm of a cascade-parallel recurrent neural network. *Sensors*, *20*(6), 1576. https://doi.org/10.3390/s20061576

Zhu, W., Beroza, G. C., & Ross, Z. E. (2019). PhaseNet: A deep-neural-network-based seismic arrival-time picking method. *Geophysical Journal International*, *216*(1), 261–273. https://doi.org/10.1093/gji/ggy423

Zou, Q., Jiang, H., Dai, K., Yao, Y., Chen, L., & Yao, D. (2019). A new approach to assess landslide susceptibility based on slope failure mechanisms in susceptibility model comparison in southeastern China. *Catena*, *182*, 104090. https://doi.org/10.1016/j.catena.2019.104090